Leptonic Jet Models of Blazars: Broadband Spectra and Spectral Variability

Markus Böttcher*

*Space Physics and Astronomy Department
Rice University, MS 108
6100 S. Main Street
Houston, TX 77005 - 1892
USA

Abstract. The current status of leptonic jet models for gamma-ray blazars is reviewed. Differences between the quasar and BL-Lac subclasses of blazars may be understood in terms of the dominance of different radiation mechanisms in the gamma-ray regime. Spectral variability patterns of different blazar subclasses appear to be significantly different and require different intrinsic mechanisms causing gamma-ray flares. As examples, recent results of long-term multiwavelength monitoring of PKS 0528+134 and Mrk 501 are interpreted in the framework of leptonic jet models. A simple quasi-analytic toy model for broadband spectral variability of blazars is presented.

INTRODUCTION

Recent high-energy detections and simultaneous broadband observations of blazars, determining their spectra and spectral variability, are posing strong constraints on currently popular jet models of blazars. 66 blazars have been detected by EGRET at energies above 100 MeV [1], the two nearby high-frequency peaked BL Lac objects (HBLs) Mrk 421 and Mrk 501 are now multiply confirmed sources of multi-GeV – TeV radiation [2–5], and the TeV detections of PKS 2155-314 [6] and 1ES 2344+514 [7] are awaiting confirmation. Most EGRET-detected blazars exhibit rapid variability [8], in some cases on intraday and even sub-hour (e. g., [9]) timescales, where generally the most rapid variations are observed at the highest photon frequencies.

The broadband spectra of blazars consist of at least two clearly distinct spectral components. The first one extends in the case of flat-spectrum radio quasars (FSRQs) from radio to optical/UV frequencies, in the case of HBLs up to soft and even hard X-rays, and is consistent with non-thermal

synchrotron radiation from ultrarelativistic electrons. The second spectral component emerges at γ-ray energies and peaks at several MeV – a few GeV in most quasars, while in the case of some HBLs the peak of this component appears to be located at TeV energies.

The bolometric luminosity of EGRET-detected quasars and some low-frequency peaked BL Lac objects (LBLs) during flares is dominated by the γ-ray emission. If this emission were isotropic, it would correspond to enormous luminosities (up to $\sim 10^{49}$ erg s^{-1}) which, in combination with the short observed timescales (implying a small size of the emission region) would lead to a strong modification of the emissivity spectra by $\gamma\gamma$ absorption, in contradiction to the observed smooth power-laws at EGRET energies. This has motivated the concept of relativistic beaming of radiation emitted by ultrarelativistic particles moving at relativistic bulk speed along a jet (for a review of these arguments, see [10]). While it is generally accepted that blazar emission originates in relativistic jets, the radiation mechanisms responsible for the observed γ radiation are still under debate. It is not clear yet whether in these jets protons are the primarily accelerated particles, which then produce the γ radiation via photo-pair and photo-pion production, followed by π^0 decay and synchrotron emission by secondary particles (e. g., [11]), or electrons (and positrons) are accelerated directly and produce γ-rays in Compton scattering interactions with the various target photon fields in the jet [12–15].

In this review, I will describe the current status of blazar models based on leptons (electrons and/or pairs; in the following, the term "electrons" refers to both electrons and positrons) as the primary constituents of the jet which are responsible for the γ-ray emission. Hadronic jet models are discussed in a separate paper by J. Rachen [16]. In Section 2, I will give a description of the model and discuss the different γ-ray production mechanisms and their relevance for different blazar classes. In Section 3, I will review recent progress in understanding intrinsic differences between different blazar classes and present state-of-the-art model calculations, using a leptonic jet model, to undermine the general theoretical concept. In Section 4, I will discuss broadband spectral variability of individual blazars and their interpretation in the framework of leptonic jet models. A simple quasi-analytical toy model for blazar broadband spectral variability will be presented in section 5.

MODEL DESCRIPTION AND RADIATION MECHANISMS

The basic geometry of leptonic blazar jet models is illustrated in Fig. 1. At the center of the AGN, an accretion disk around a supermassive, probably rotating, black hole is powering a relativistic jet. Along this pre-existing jet structure, occasionally blobs of ultrarelativistic electrons are ejected at relativistic bulk velocity.

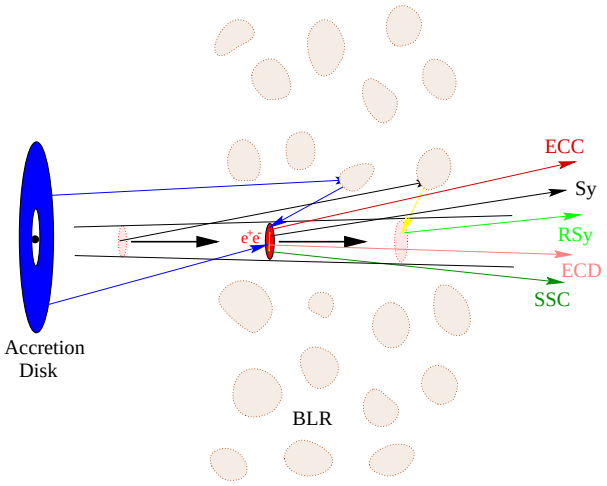

FIGURE 1. Illustration of the model geometry and the relevant γ radiation mechanisms for leptonic jet models.

The electrons are emitting synchrotron radiation, which will be observable at IR – UV or even X-ray frequencies, and hard X-rays and γ-rays via Compton scattering processes. Possible target photon fields for Compton scattering are the synchrotron photons produced within the jet (the SSC process, [12,17,18]), the UV – soft X-ray emission from the disk — either entering the jet directly (the ECD [External Comptonization of Direct disk radiation] process; [13,19]) or after reprocessing at the broad line regions or other circumnuclear material (the ECC [External Comptonization of radiation from Clouds] process; [14,20,21]), or jet synchrotron radiation reflected at the broad line regions (the RSy [Reflected Synchrotron] mechanism; [22–24]).

The relative importance of these components may be estimated by comparing the energy densities of the respective target photon fields. Denoting by u'_B the co-moving energy density of the magnetic field, the energy density of the synchrotron radiation field, governing the luminosity of the SSC component, may be estimated by $u'_{sy} \approx u'_B \, \tau_T \, \gamma_e^2$, where $\tau_T = n'_{e,B} \, R'_B \, \sigma_T$ is the Thomson depth of the relativistic plasma blob and γ_e is the average Lorentz factor of electrons in the blob. The SSC spectrum exhibits a broad hump without strong spectral break, peaking around $\langle\epsilon\rangle_{SSC} \approx (B'/B_{cr}) \, D \, \gamma_e^4 \approx \langle\epsilon\rangle_{sy} \, \gamma_e^2$, where B' is the co-moving magnetic field, $B_{cr} = 4.414 \cdot 10^{13}$ G, and $D = (\Gamma \, [1 - \beta_\Gamma \cos\theta_{obs}])^{-1}$ is the Doppler factor associated with the bulk motion of the blob. Throughout this paper, all photon energies are described by the dimensionless quantity $\epsilon = h\nu/(m_e c^2)$.

If the blob is sufficiently far from the central engine of the AGN so that the accretion disk can be approximated as a point source of photons, its photon energy density (in the co-moving frame) is $u'_D \approx L_D/(4\pi \, z^2 \, c \, \Gamma^2)$, where L_D is the accretion disk luminosity, and z is the height of the blob above the accretion disk. The ECD spectrum can exhibit a strong spectral break, depending

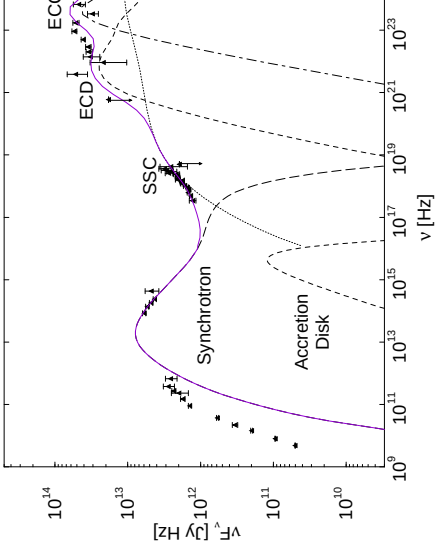

r]

FIGURE 2. Fit to the simultaneous broadband spectrum of the FSRQ 3C279 during its very bright γ-ray flare in September 1991. See [29] for model parameters.

on the existence of a low-energy cutoff in the electron distribution function, and peaks at $\langle\epsilon\rangle_{ECD} \approx \langle\epsilon\rangle_D \, (D/\Gamma) \, \gamma_e^2$, where $\langle\epsilon\rangle_D$ is the average photon energy of the accretion disk radiation (typically of order 10^{-5} for Shakura-Sunyaev type accretion disks [25] around black holes of $\sim 10^8$ – $10^{10} \, M_\odot$).

Part of the accretion disk and the synchrotron radiation will be reprocessed by circumnuclear material in the broad line region and can re-enter the jet. Since this reprocessed radiation is nearly isotropic in the rest-frame of the AGN, it will be strongly blue-shifted into the rest-frame of the relativistically moving plasma blob. Thus, assuming that a fraction a_{BLR} of the radiation is rescattered into the jet trajectory, we find for the energy density of rescattered accretion disk photons: $u'_{ECC} \approx L_D \, a_{BLR} \, \Gamma^2 / (4\pi \, \langle r\rangle_{BLR}^2 \, c)$, where $\langle r\rangle_{BLR}$ is the average distance of the BLR material from the central black hole. The ECC photon spectrum peaks around $\langle\epsilon\rangle_{ECC} \approx \langle\epsilon\rangle_D \, D \, \Gamma \, \gamma_e^2 \approx \langle\epsilon\rangle_{ECD} \, \Gamma^2$.

For the synchrotron mirror mechanism, additional constraints due to light travel time effects need to be taken into account in order to estimate the reflected synchrotron photon energy density (for a detailed discussion see [24]), which is well approximated by $u'_{RSy} \approx u'_{sy} \, 4 \, \Gamma^3 \, a_{BLR} \, (R'_B/\Delta r_{BLR}) \, (1 - 2 \, \Gamma \, R'_B/z)$, where Δr_{BLR} is a measure of the geometrical thickness of the broad line region. Similar to the SSC spectrum, the RSy spectrum does not show a strong spectral break. It peaks around $\langle\epsilon\rangle_{RSy} \approx (B'/B_{cr}) \, D \, \Gamma^2 \, \gamma_e^4 \approx \langle\epsilon\rangle_{SSC} \, \Gamma^2$.

TRENDS BETWEEN DIFFERENT BLAZAR CLASSES

There appears to be a more or less continuous sequence in the broadband spectral properties of blazars, ranging from FSRQs over LBLs to HBLs, which was first presented in a systematic way in [26]. While in FSRQs the synchrotron and γ-ray peaks are typically located at infrared and MeV – GeV

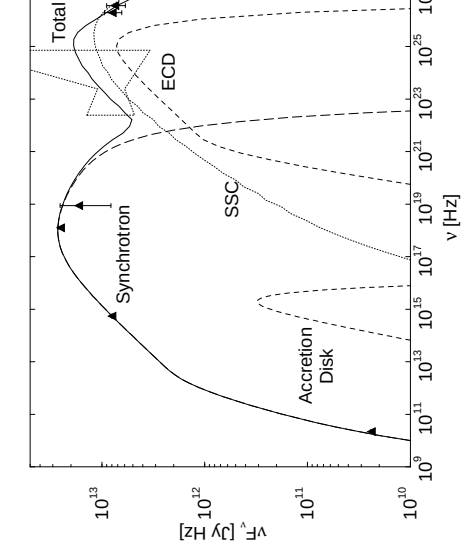

r]

FIGURE 3. Fit to a weekly-averaged broadband spectrum of the extreme HBL Mrk 501 during a high γ-ray state centered on MJD 50564 in 1997. The dotted "bow-tie" curve indicates the highest flux ever measured by EGRET, which provides an upper limit for the possible contribution of external Comptonization. See [32] for model parameters.

energies, respectively, they are shifted towards higher frequencies in BL Lacs, occurring at medium to even hard X-rays and at multi-GeV – TeV energies in some HBLs. The bolometric luminosity of FSRQs is — at least during γ-ray high states — strongly dominated by the γ-ray emission, while in HBLs the relative power outputs in synchrotron and γ-ray emission are comparable.

Detailed modeling of several blazars has indicated that this sequence appears to be related to the relative contribution of the external Comptonization mechanisms ECD and ECC to the γ-ray spectrum. While most FSRQs are successfully modelled with external Comptonization models (e. g., [21,27–29]), the broadband spectra of HBLs are consistent with pure SSC models (e. g., [30–32]). BL Lacertae, a LBL, appears to be intermediate between these two extremes, requiring an external Comptonization component to explain the EGRET spectrum [33,34]. Figs. 2 and 3 illustrate detailed modeling results of two objects located at opposite ends of this sequence of blazars, using the jet radiation transfer code described in [15,34].

A physical interpretation of this sequence in the framework of a unified jet model for blazars was given in [35]. Assume that the average energy of electrons, γ_e, is determined by the balance of an energy-independent acceleration rate $\dot{\gamma}_{acc}$ and radiative losses, $\dot{\gamma}_{rad} \approx -(4/3)\, c\, \sigma_T\, (u'/m_e c^2)\, \gamma^2$, where the target photon density u' is the sum of the sources intrinsic to the jet, $u'_B + u'_{sy}$ plus external photon sources, $u'_{ECD} + u'_{ECC} + u'_{RSy}$. The average electron energy will then be $\gamma_e \propto (\dot{\gamma}_{acc}/u')^{1/2}$. If one assumes that the properties determining the acceleration rate of relativistic electrons do not vary significantly between different blazar subclasses, then an increasing energy density of the external radiation field will obviously lead to a stronger radiation component due to external Comptonization, but also to a decreasing average electron energy γ_e, implying that the peak frequencies of both spectral components are displaced

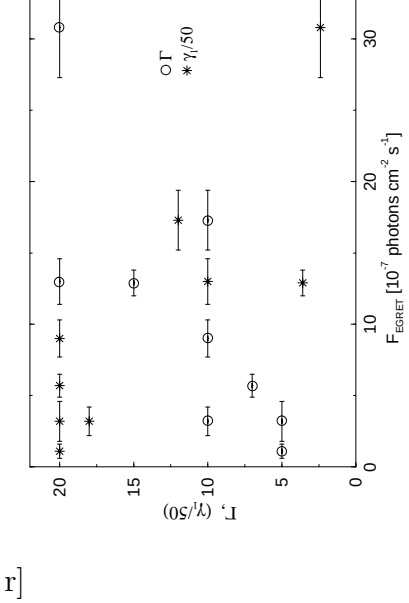

r]

FIGURE 4. The dependence of the fit parameters Γ and γ_1 (low-energy cut-off of the electron distribution) on the EGRET flux for fits to simultaneous broadband spectra of PKS 0528+134 (see [28]).

towards lower frequencies.

SPECTRAL VARIABILITY OF BLAZARS

Between flaring and non-flaring states, blazars show very distinct spectral variability. Not only does the emission at the highest frequencies generally vary on the shortest time scales, but also the flaring amplitudes are significantly different among different wavelength bands. FSRQs often show spectral hardening of their γ-ray spectra during γ-ray flares (e. g., [36,39,40]), and the flaring amplitude in γ-rays is generally larger than in all other wavelength bands. The concept of multi-component γ-ray spectra of quasars, as first suggested for PKS 0528+134 in [36], offers a plausible explanation for this spectral variability due to the different beaming patterns of different radiation mechanisms, as pointed out in [37]. This has been applied to PKS 0528+134 in [38] and [28].

The results of [28] indicate that γ-ray flaring states of PKS 0528+134 are consistent with an increasing bulk Lorentz factor Γ of ejected jet material, while at the same time the low-energy cutoff γ_1 of the electron distribution injected into the jet is lowered. This is in agreement with the physical picture that due to an increasing Γ, the quasi-isotropic external photon field is more strongly Lorentz boosted into the blob rest frame, leading to stronger external Compton losses, implying a lower value of γ_1. The external Compton γ-ray components depend much more strongly on the bulk Lorentz factor than the synchrotron and SSC components do. This leads naturally to a hardening of the γ-ray spectrum, if the SSC mechanisms plays an important or even dominant role in the X-ray — soft γ-ray regime, while external Comptonization is the dominant radiation mechanism at higher γ-ray energies. The results of

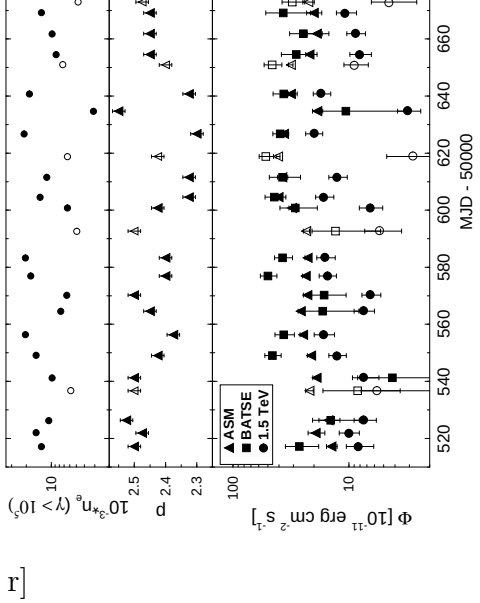

FIGURE 5. Temporal variation of the fit parameters $n_e(\gamma > 10^5)$ (density of high-energy electrons) and p (spectral index of injected electron distribution) compared to the weekly averaged light curves from RXTE ASM, BATSE and HEGRA (see [32]).

this study on PKS 0528+134 are discussed in more detail in [41].

While this flaring mechanism is plausible for FSRQs, short-timescale, correlated X-ray and γ-ray flares of the HBLs Mrk 421 and Mrk 501 [30,31] and synchrotron flares of other HBLs (e. g., PKS 2155-304, [42,43]) have been explained successfully in the context of SSC models where flares are related to an increase of the maximum electron energy, γ_2, and a hardening of the electron spectrum. How the spectral evolution in synchrotron flares can be used to constrain the magnetic field and the physics of injection and acceleration of relativistic pairs, has been described in detail in the previous talk by R. Sambruna [44].

Comparing detailed spectral fits to weekly averaged broadband spectra of Mrk 501 [32] over a period of 6 months, we have found that TeV and hard X-ray high states on intermediate timescales are consistent with a hardening of the electron spectrum (decreasing spectral index) and an increasing number density of high-energy electrons, while the value of γ_2 has only minor influence on the weekly averaged spectra. Fig. 5 shows how the spectral index of the injected electron distribution and the density of high-energy electrons resulting from our fits are varying in comparison to the RXTE ASM, BATSE, and HEGRA 1.5 TeV light curves. For a more detailed discussion of this analysis see [45].

These variability studies seem to indicate that due to the different dominant γ radiation mechanisms in quasars and HBLs also the physics of γ-ray flares and extended high states is considerably different. While in FSRQs the γ-ray emission and its flaring behavior appears to be dominated by conditions of the external radiation field, this influence is unimportant in the case of HBLs where emission lines are very weak or absent, implying that the BLR might be very dilute, leading to a very weak external radiation field, which becomes negligible compared to the synchrotron radiation field intrinsic to the jet.

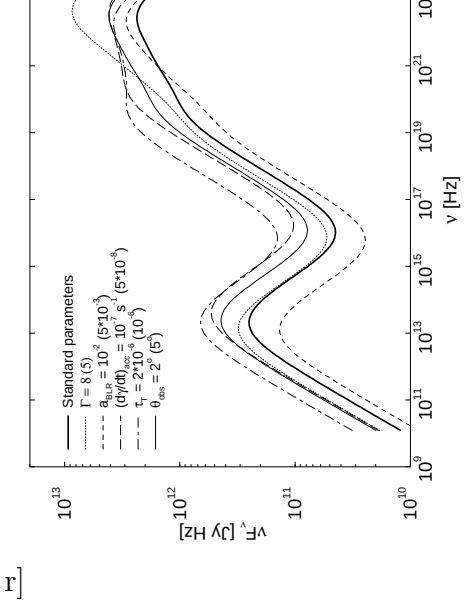

r]

FIGURE 6. Thick solid curve: Toy model calculation representative of the broadband spectrum of PKS 0528+134. Parameters: $\Gamma = 5$, $\theta_{obs} = 5^o$, $\dot{\gamma}_{acc} = 5 \cdot 10^{-8}$ s^{-1}, $L_D = 6 \cdot 10^{46}$ erg s^{-1}, $\langle\epsilon\rangle_D = 10^{-5}$, $a_{BLR} = 5 \cdot 10^{-3}$, $z = 2 \cdot 10^{17}$ cm, $R'_B = 3 \cdot 10^{16}$ cm, $\tau_T = 10^{-6}$. For the other curves, a single parameter, as indicated by the label, has been changed (value of the original calculation in parantheses).

A TOY MODEL FOR SPECTRAL VARIABILITY

On the basis of the estimates of the photon energy densities of the various radiation fields and the peak energies of the diverse radiation components given in Section 2, one can develop a very simple, quasi-analytic toy model which allows us to study the influence of parameter variations on the predicted broadband spectrum of a blazar. For construction of this toy model, I assume that the magnetic field within the jet is in equipartition with the ultrarelativistic electrons, and that the light-travel time effects affecting the efficiency of the synchrotron mirror mechanism can be parametrized by a correction factor $f_{ltt} \lesssim 0.1$ so that $u'_{RSy} \approx u'_{sy}\, a_{BLR}\, \Gamma^3\, f_{ltt}$. Then, the entire broadband spectrum, accounting for all synchrotron and inverse-Compton components, is determined by 9 parameters: Γ, θ_{obs}, $\dot{\gamma}_{acc}$, L_D, $\langle\epsilon\rangle_D$, a_{BLR}, the scale height z of energy dissipation in the jet, R'_B, and τ_T. In most cases, several of these parameters can be constrained by independent observations. The radiation spectra of each individual component are approximated by double power-laws with a smooth transition.

The thick solid curve in Fig. 6 shows a toy model calculation with the location of peak frequencies and the relative contributions of the γ radiation components as found in our fits to PKS 0528+134 based on detailed simulations [28]. The hard X-ray to soft γ-ray spectrum below ~ 1 MeV is dominated by the SSC mechanism, while at higher energies, the ECC mechanism is dominant. The other curves in Fig. 6 indicate the effect of single parameter changes on the broadband spectrum which could be thought of as the cause of flares at γ-ray energies.

From Fig. 6, one can see that an increasing bulk Lorentz factor leads to

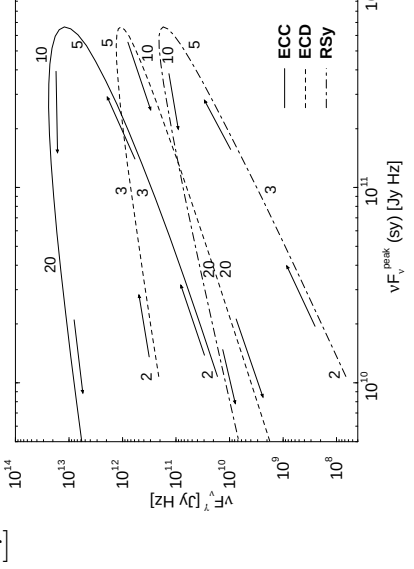

r]

FIGURE 7. Variation of the power output in synchrotron and the external Comptonization components if the bulk Lorentz factor Γ is the only parameter changing during a flare. The numbers along the curves are the respective values of Γ at that point, and the arrows indicate the sense of evolution if Γ is increasing.

a strong flare at γ-ray energies, while only moderate flaring at infrared and X-ray frequencies results (dotted curve). A shift of the synchrotron peak towards lower frequencies is predicted [46]. If the BLR albedo a_{BLR} increases (short-dashed curve), the result is a slight increase in the power output at high-energy γ-rays, while due to enhanced external-Compton cooling the flux in the synchrotron and SSC components even decreases. An increased acceleration rate $\dot{\gamma}_{acc}$ (long-dashed curve), leads to a strong synchrotron and SSC flare, where the largest variability amplitude is expected at MeV energies, while only moderate variability at higher frequencies is predicted. If the density of relativistic electrons in the blob increases during a flare (dot-dashed curve), the variability amplitude is again predicted to be largest at MeV energies and the peak frequencies of all components are expected to be shifted slightly towards lower frequencies. A decreasing observing angle — which could be a consequence of a bending jet — leads to a shift of the entire broadband spectrum towards higher fluxes and slightly higher peak frequencies.

Obviously, definite conclusions can not be drawn from this simplistic toy-model analysis. However, it may support previous results that an increasing bulk Lorentz factor is a viable and plausible explanation for the spectral variability observed in PKS 0528+134 and possibly also in other FSRQs.

Fig. 7 illustrates the variation of the power output in the different external Compton γ-ray components with respect to the synchrotron component, if Γ is the only parameter changing during a γ-ray flare. Most notably, a very steep relation between $\nu F_\nu^{peak}(sy)$ and $\nu F_\nu^{peak}(ECC)$ is predicted for values of the Lorentz factor close to the critical Γ, at which the observer is looking at the superluminal angle. This dependence can be significantly steeper than quadratic, $\Delta\nu F_\nu^{peak}(sy) \propto \left[\Delta\nu F_\nu^{peak}(ECC)\right]^\alpha$ with $\alpha > 2$, which has recently been observed in the prominent 1996 flare of 3C279 [40].

REFERENCES

1. Hartman, R. C., et al., *ApJ*, in press (1999a).
2. Punch, M., et al., *Nature*, **358**, 477 (1992).
3. Petry, D., et al., *A&A*, **311**, L13 (1996).
4. Quinn, J., et al., 1996, *ApJ*, **456**, L83 (1996).
5. Bradbury, S. M., et al., 1997, *A&A*, **320**, L5 (1997).
6. Chadwick, P. M., et al., *ApJ*, in press (1999).
7. Catanese, M., et al., *ApJ*, **501**, 616 (1998).
8. Mukherjee, R., et al., *ApJ*, **490**, 116 (1997).
9. Gaidos, J. A., et al., *Nature*, **383**, 319 (1996).
10. Schlickeiser, R., *Space Sci. Rev.* **75**, 299 (1996).
11. Mannheim, K., *A&A*, **269**, 67 (1993).
12. Marscher, A. P., & Gear, W. K., *ApJ*, **298**, 114 (1985).
13. Dermer, C. D., Schlickeiser, R., & Mastichiadis, A., *A&A*, **256**, L27 (1992).
14. Sikora, M., Begelman, MM. C., & Rees, M. J, *ApJ*, **421**, 153 (1994).
15. Böttcher, M., Mause, H., & Schlickeiser, R., *A&A*, **324**, 395 (1997).
16. Rachen, J., these proceedings (1999).
17. Maraschi, L., Ghisellini, G., & Celotti, A., *ApJ*, **397**, L5 (1992).
18. Bloom, S. D., & Marscher, A. P., *ApJ*, **461**, 657 (1996).
19. Dermer, C. D., & Schlickeiser, R., *ApJ*, **416**, 458 (1993).
20. Blandford, R. D., & Levinson, A., *ApJ*, **441**, 79 (1995).
21. Dermer, C. D., Sturner, S. J., & Schlickeiser, R., *ApJS*, **109**, 103 (1997).
22. Ghisellini, G., & Madau, P., *MNRAS*, **280**, 67 (1996).
23. Bednarek, W., *A&A*, **342**, 69 (1998).
24. Böttcher, M., & Dermer, C. D., *ApJ*, **501**, L51 (1998).
25. Shakura, N. I., & Sunyaev, R. A., *A&A*, **24**, 337 (1973).
26. Fossati, G., et al., *MNRAS*, **289**, 136 (1997).
27. Sambruna, R., et al., *ApJ*, **474**, 639 (1997).
28. Mukherjee, R., et al., *ApJ*, **527**, in press (1999).
29. Hartman, R. C., et al., in preparation (1999b).
30. Mastichiadis, A., & Kirk, J. G., *A&A*, **320**, 19 (1997).
31. Pian, E., et al., *ApJ*, **492**, L17 (1998).
32. Petry, D., et al., *ApJ*, submitted (1999).
33. Madejski, G., et al., *ApJ*, **521**, 145 (1999).
34. Böttcher, M., & Bloom, S. D., *AJ*, submitted (1999).
35. Ghisellini, G., et al., *MNRAS*, **301**, 451 (1998).
36. Collmar, W., et al., *A&A*, **328**, 33 (1997).
37. Dermer, C. D., *ApJ*, **446**, L63 (1995).
38. Böttcher, M., & Collmar, W., *A&A*, **329**, L57 (1998).
39. Hartman, R. C., et al., *ApJ*, **461**, 698 (1996).
40. Wehrle, A. E., et al., *ApJ*, **497**, 178 (1998).
41. Mukherjee, R., & Böttcher, M., these proceedings (1999).
42. Georganopoulos, M., & Marscher, A. P., *ApJ*, **506**, L11 (1998).
43. Kataoka, J., et al. *ApJ*, in press (1999).

44. Sambruna, R., these proceedings (1999).
45. Böttcher, M., Petry, D., & Connaughton, V., these proceedings (1999).
46. Böttcher, M., *ApJ*, **515**, L21 (1999).

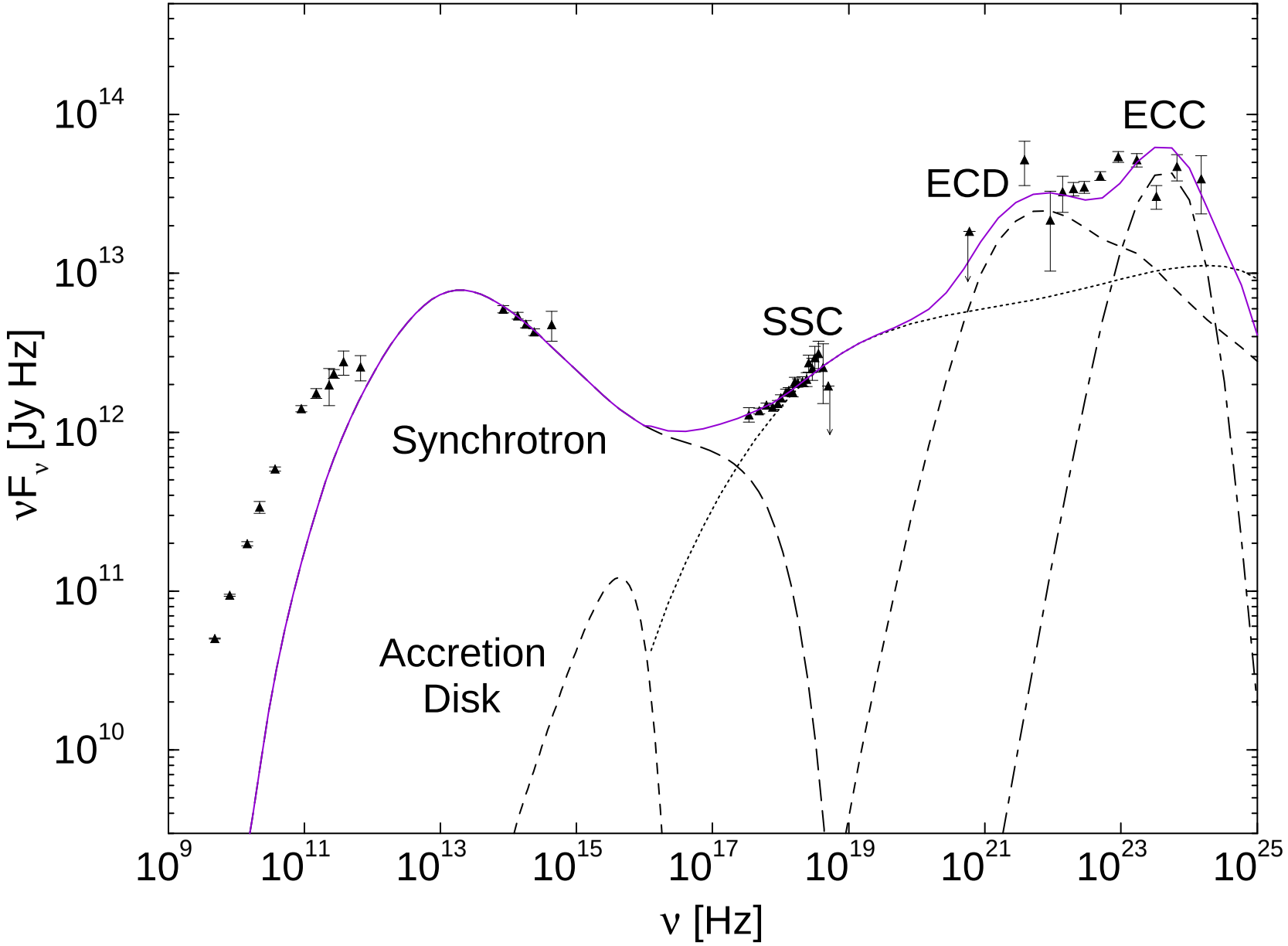
ECC
ECD
SSC
Synchrotron
Accretion
Disk
νF_ν [Jy Hz]
ν [Hz]
10^14
10^13
10^12
10^11
10^10
10^9
10^11
10^13
10^15
10^17
10^19
10^21
10^23
10^25

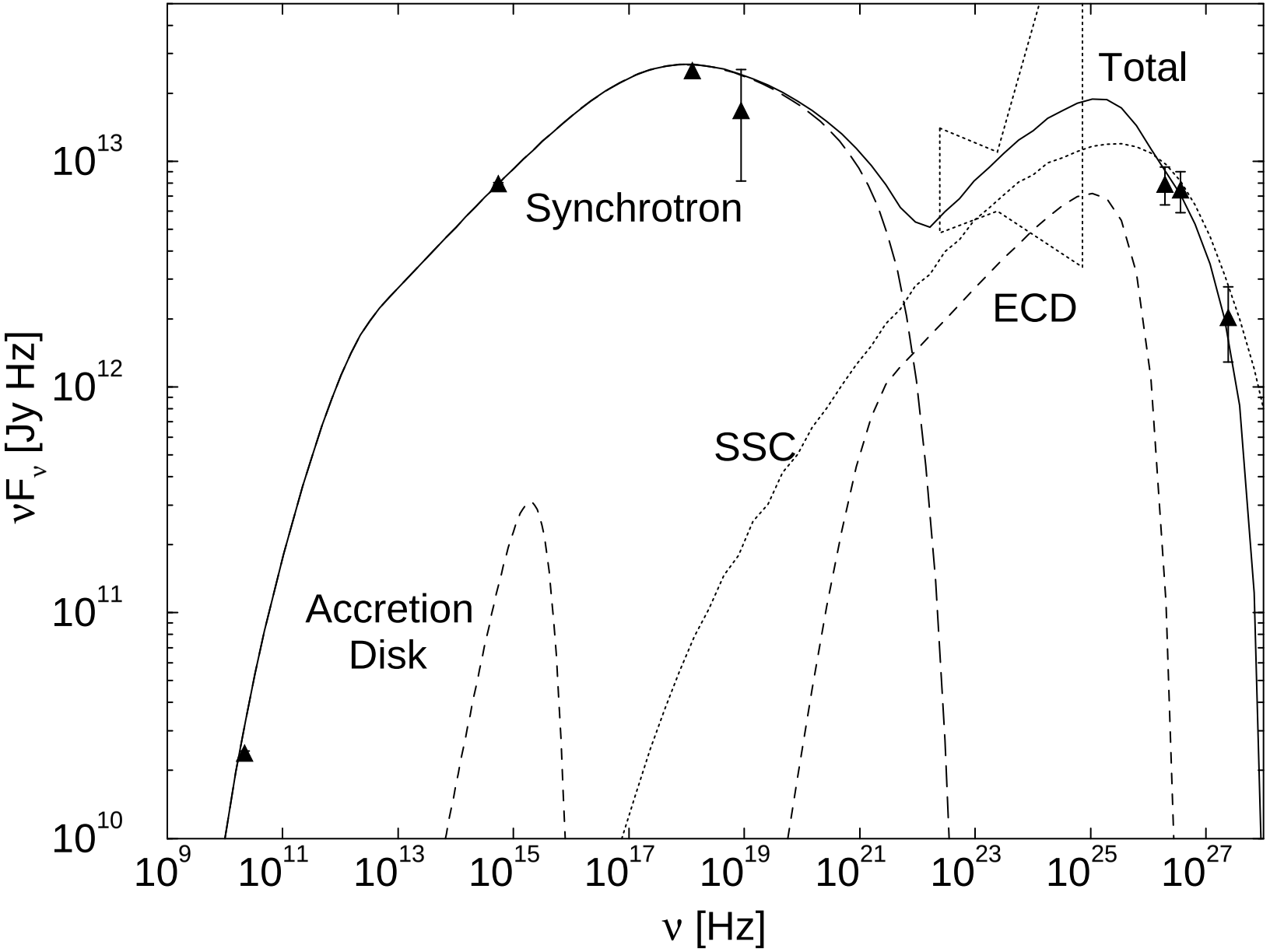
Total
Synchrotron
ECD
SSC
Accretion
Disk
10^{13}
10^{12}
10^{11}
10^{10}
νF_ν [Jy Hz]
10^{9}
10^{11}
10^{13}
10^{15}
10^{17}
10^{19}
10^{21}
10^{23}
10^{25}
10^{27}
ν [Hz]

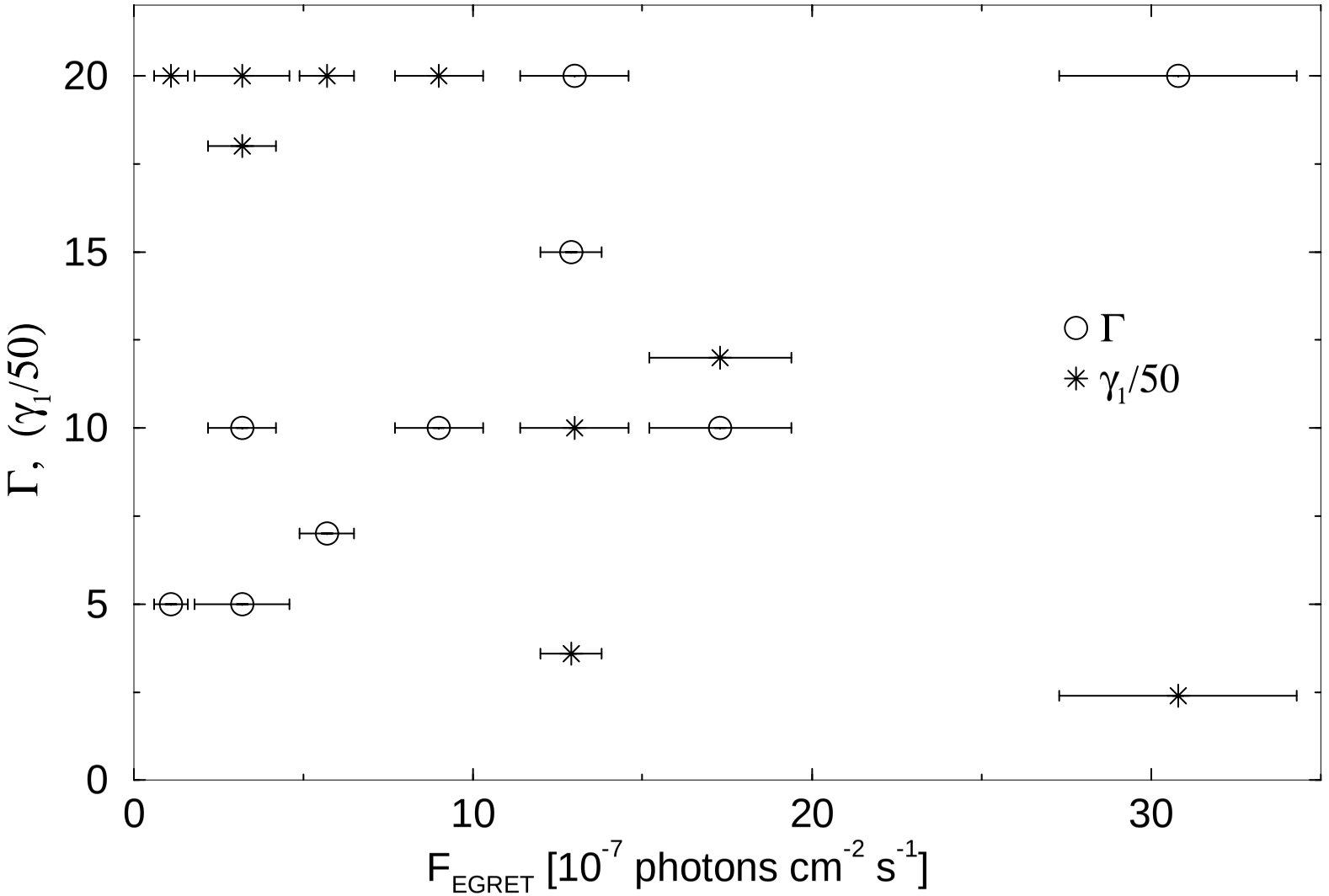
20
15
10
5
0
0
10
20
30
Γ, (γ1/50)
F_EGRET [10^-7 photons cm^-2 s^-1]
○ Γ
✳ γ1/50

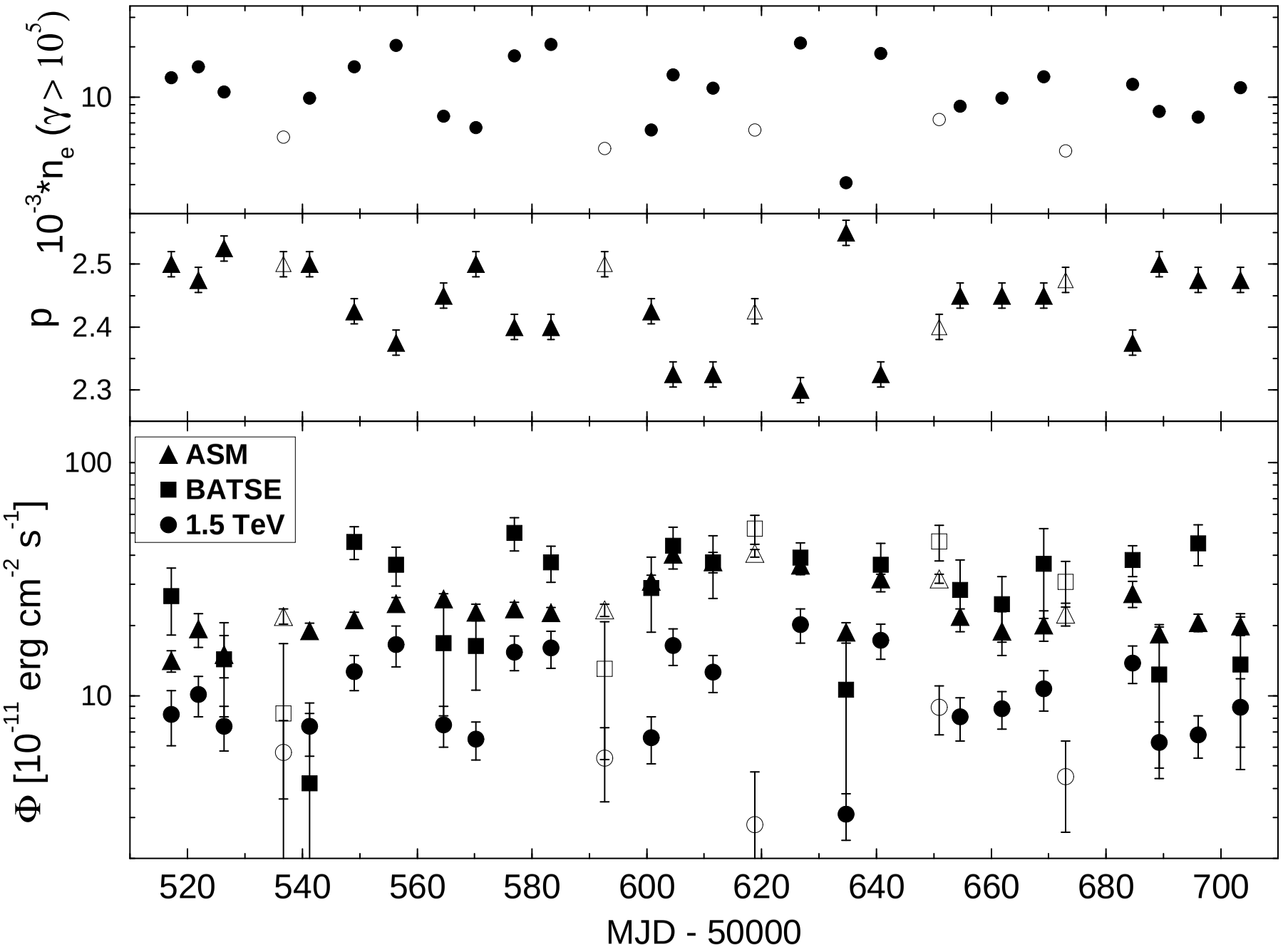
10
$10^{-3}*n_e\ (\gamma > 10^5)$
2.5
2.4
2.3
p
ASM
BATSE
1.5 TeV
100
10
$\Phi\ [10^{-11}\ erg\ cm^{-2}\ s^{-1}]$
520
540
560
580
600
620
640
660
680
700
MJD - 50000

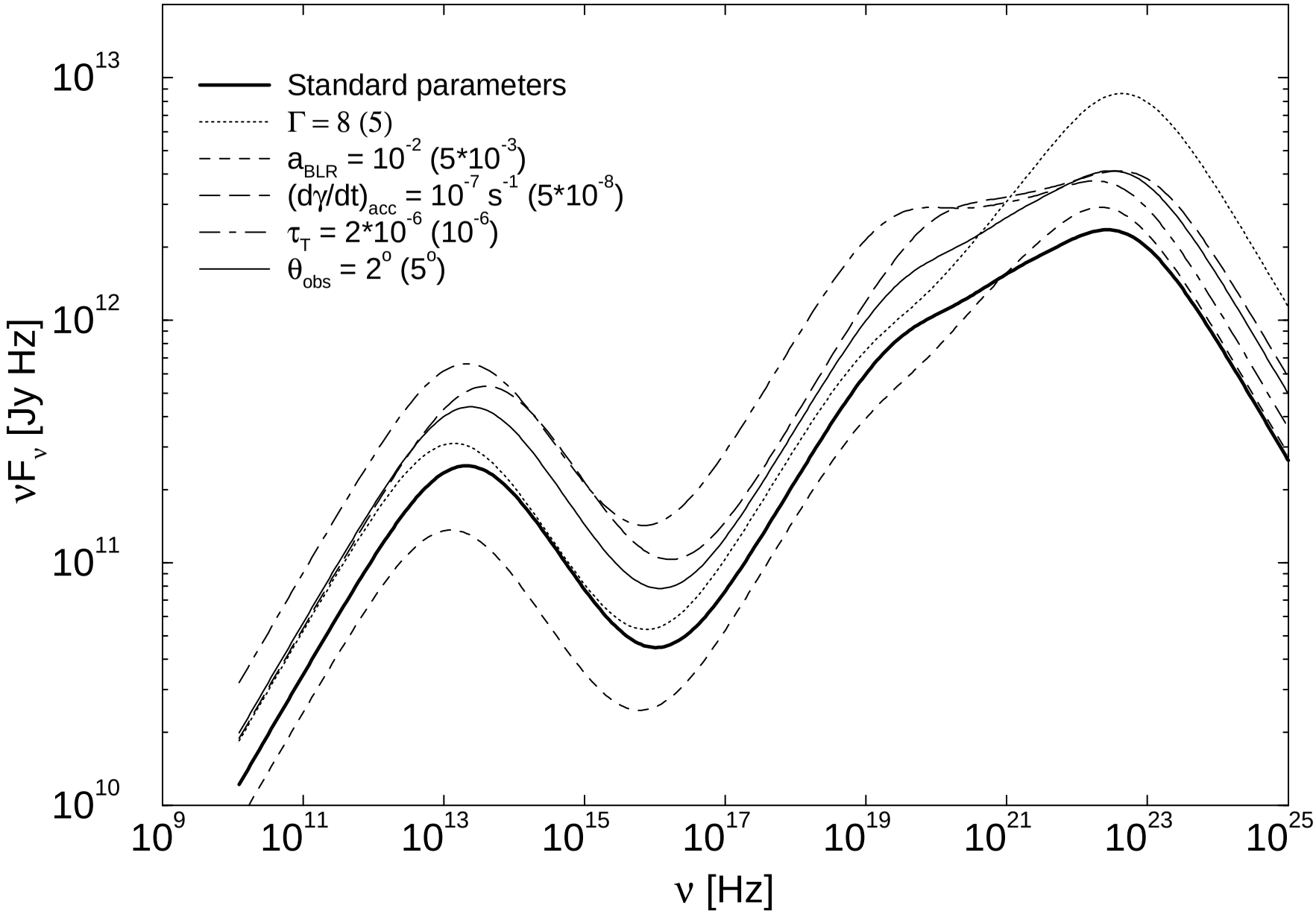
Standard parameters
Γ = 8 (5)
a_BLR = 10^-2 (5*10^-3)
(dγ/dt)_acc = 10^-7 s^-1 (5*10^-8)
τ_T = 2*10^-6 (10^-6)
θ_obs = 2° (5°)
νF_ν [Jy Hz]
ν [Hz]
10^13
10^12
10^11
10^10
10^9
10^11
10^13
10^15
10^17
10^19
10^21
10^23
10^25

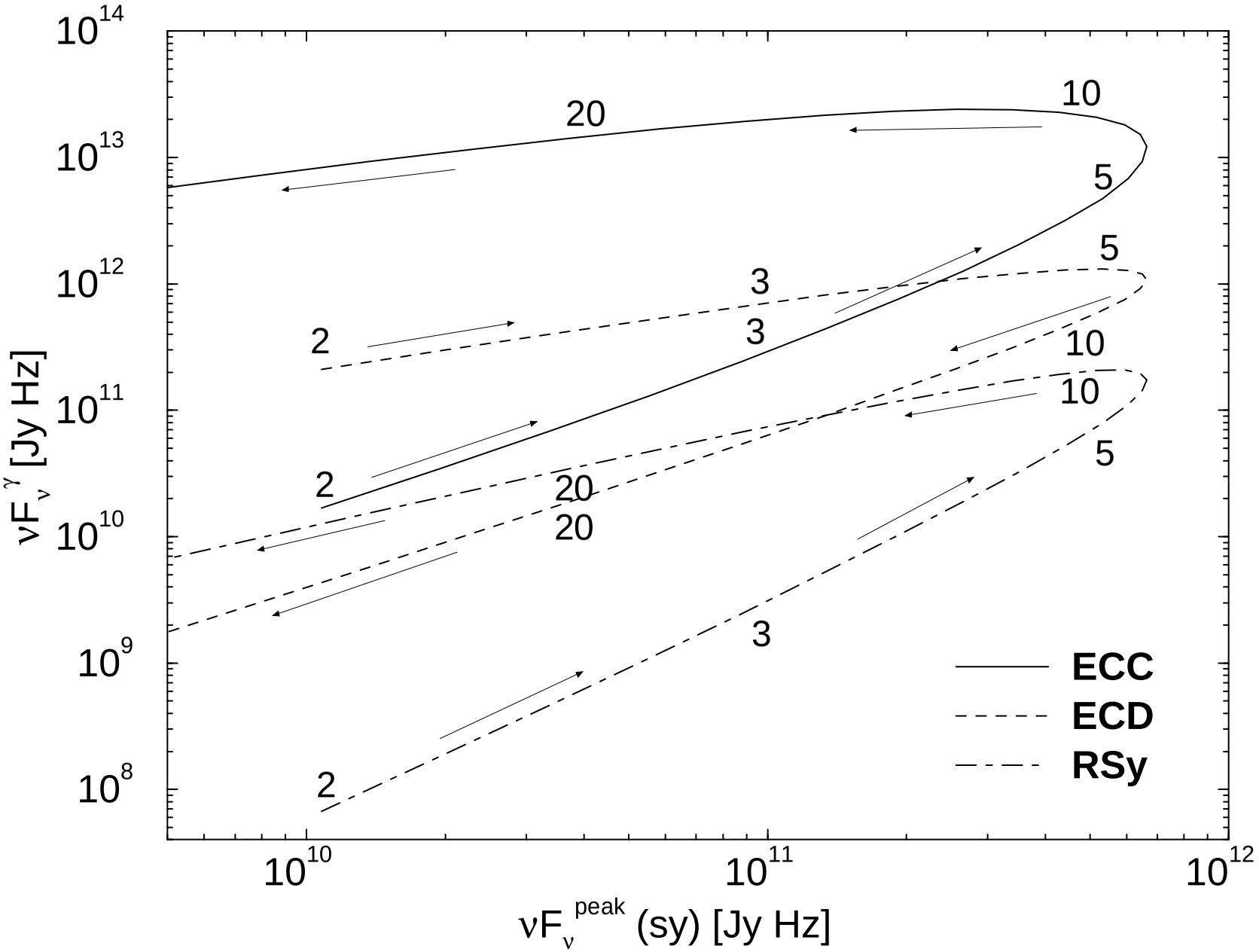
10^{14}
10^{13}
10^{12}
10^{11}
10^{10}
10^{9}
10^{8}
νF_ν^{γ} [Jy Hz]
10^{10}
10^{11}
10^{12}
νF_ν^{peak} (sy) [Jy Hz]
20
10
5
3
2
ECC
ECD
RSy